NUCL SCI TECH (2020) 31:13
https://doi.org/10.1007/s41365-020-0722-z

Collection efficiency of a monitor parallel plate ionization chamber for pencil beam scanning proton therapy

Rong-Cheng Han[1,2] · **Yong-Jiang Li**[3] · **Yue-Hu Pu**[3,4]

Received: 26 July 2019 / Revised: 3 December 2019 / Accepted: 3 December 2019 / Published online: 24 January 2020

Abstract The collection efficiency of monitor parallel plate ionization chambers is the main uncertainty in the beam control of pencil beam scanning systems. Existing calculation methods for collection efficiency in photon or passive scattering proton systems have not considered the characteristics of non-uniform charge density in pencil beam scanning systems. In this study, Boag's theory was applied to a proton pencil beam scanning system. The transverse distribution of charge density in the ionization chamber was considered to be a Gaussian function and an analytical solution was derived to calculate collection efficiency in the beam spot area. This calculation method is called the integral method and it was used to investigate the effects of beam parameters on collection efficiency. It was determined that collection efficiency is positively correlated with applied voltage, beam size, and beam energy, but negatively correlated with beam current intensity. Additionally, it was confirmed that collection efficiency is improved when the air filling the monitor parallel plate ionization chamber is replaced with nitrogen.

✉ Yue-Hu Pu
puyuehu@sinap.ac.cn

[1] Shanghai Institute of Applied Physics, Chinese Academy of Sciences, Shanghai 201800, China

[2] University of Chinese Academy of Sciences, Beijing 100049, China

[3] Shanghai APACTRON Particle Equipment Co. Ltd, Shanghai 201800, China

[4] Shanghai Advanced Research Institute, Chinese Academy of Sciences, Shanghai 201210, China

Keywords Collection efficiency · Monitor ionization chamber · Pencil beam scanning · Proton therapy

1 Introduction

The history of proton therapy began in 1946 when Robert Wilson published a seminal paper in which he proposed the use of accelerator-produced beams from protons for treating tumors in humans [1]. Based on characteristic depth-dose distributions with Bragg peaks, proton therapy has been widely used in cancer therapy for the past few decades. There are two main delivery techniques that are currently used for proton therapy: passive scattering and pencil beam scanning systems (also called active scanning systems). Passive scattering systems use scattering devices in a treatment delivery nozzle to spread beams laterally and a range modulation wheel or ridge filter to create a spread-out Bragg peak in the target volume. Pencil beam scanning systems use magnetic fields to scan proton beams laterally across the target and combine this capability with the ability to change the beam energy, facilitating conformality in three dimensions. Pencil beam scanning systems are advantageous in that they can deliver high and conformal doses to targets while minimizing doses to nearby organs at risk [2, 3] (OARs). Therefore, most proton therapy facilities under construction have adopted pencil beam scanning systems. Such systems have also been adopted at the Shanghai Advanced Proton Therapy (SAPT) facility [4–6]. Since the pencil beam scanning system individually weights each beam spot to superpose a homogeneous dose distribution on the target, high-accuracy dose measurement and complex computerized control systems are required.

As the most common, convenient, and precise dose-measuring instruments in radiotherapy dosimetry [7, 8], ionization chambers are typically used as reference instruments for clinical ion beams [9, 10]. According to international dosimetry protocols, such as IAEA TRS-398 [11], ICRU34 [12], and AAPM-TG51 [13], the response of an ionization chamber must be corrected based on the ion collection efficiency f, which represents the effects of incomplete collection of charges as a result of ion recombination in the chamber gas cavity. Ion recombination mechanisms can be classified as initial recombination and volume recombination (or general recombination) [14]. Initial recombination occurs along the track of individual charge particles and can be assumed to be independent of the ionization current but is dependent on the ionization density within the track. Therefore, initial recombination is more significant in high- LET (linear energy transfer) beams than in low-LET beams [15–17]. Volume recombination, which results from diffusion and the electrostatic attraction of charge carriers distributed homogeneously within the ionization volume, occurs between ions generated in different ionization tracks [18].

Numerous studies have focused on evaluating and verifying collection efficiency based on ion recombination in photons and electrons [19–21]. Additionally, interest in studying ion recombination in proton beam and carbon beam dosimetry has increased recently. Previous studies on the ionization chamber collection efficiency of passive scattering systems have indicated that the recombination effect is small and can be ignored. Palmans [22] determined that recombination factors did not exceed 0.2% for four plane-parallel ionization chambers in the scattering proton system at the Université Catholique de Louvain by using the two-voltage-method recommended by the IAEA TRS-398 protocol. Palmans also measured recombination corrections at the Clatterbridge Center of Oncology by using data collected at different dose rates in a low-energy clinical scattering proton beam. Palmans concluded that recombination correction factors can be overestimated by up to 2% if the recommendation of TRS-398, which is only valid for pulsed beams, is followed without modification [23].

However, in the case of pencil scanning beams, the dose rate in a single proton pencil beam may be much higher than that in clinical photon and electron beams. Lorin [24] pointed out that the initial portion of recombination is negligible for a scanned proton system, but volume recombination must be corrected. Rossomme [25, 26] calculated an initial recombination factor using Jaffe's theory [15] and a volume recombination factor using Boag's theory [14]. Compared to the collection correction factor derived from experiments, Rossomme concluded that unlike studies conducted on passively scattered therapeutic particle beams, based on the high dose rates of scanning particle beams, Jaffe's theory is not sufficient for describing the ion recombination mechanism. Furthermore, ion recombination in the investigated proton pencil beams was dominated by volume recombination, which could be modeled successfully by Boag's theory. The conclusion that volume recombination effects cannot be ignored was supported by Liszka's study [27], which compared experimental collection correction factors to theoretical calculations. Tansho [28] proposed a method based on Boag's theory to account for spatially non-uniform ionized charge density when calculating volume recombination of a field chamber in a carbon-ion scanning system. Several recent publications have focused on deriving new formulas or developing open-source code to calculate ion recombination correction in pencil beam scanning proton therapy [29, 30].

Most of the studies discussed above focused on field ionization chambers, which are used for quality assurance. In a proton therapy facility, monitor parallel plate ionization chambers are installed in the treatment nozzle to perform monitoring and control during the scanning irradiation process. It is of critical importance to consider the collection efficiency of monitor parallel plate ionization chambers to ensure the accuracy of dose delivery. In this study, we only considered volume recombination for calculating collection efficiency. Based on uncertainties in dose measurement and proton beam delivery [31, 32], such as the polarity effect and the leakage doses, as well as on information from the M.D. Anderson Cancer Center [33], we considered 0.99 as the benchmark standard value for collection efficiency and used this collection efficiency value to study constraints on beam parameters.

Boag's model assumes that ionized charge density in an ionization chamber is spatially uniform, which is applicable to passive scattering systems, but not to pencil beam scanning systems based on their non-uniform charge density. We considered the non-uniform transverse distribution of charge density as a Gaussian function and applied Boag's theory to a proton pencil beam scanning system. An analytical solution was derived to calculate collection efficiency in the beam spot area. This calculation method is called the integral method and it was used to investigate the effects of beam parameters on collection efficiency. It should be noted that the collection efficiency in this work was calculated theoretically. Measurement of collection efficiency will require additional research.

The remainder of this paper is organized as follows. In Sect. 2, the basic expression for Boag's theory and the analytical solution for collection efficiency in a pencil beam scanning system are described. In Sect. 3 the correlations between collection efficiency and beam parameters, such as beam current intensity, beam size, and beam

energy, are discussed. Additional discussion and conclusions are provided in Sects. 4 and 5, respectively.

2 Methods

2.1 Boag's theory

Boag's theory is widely used to calculate the collection efficiency of ionization chambers [14–18] for both pulsed and continuous beams. Figure 1 presents the time structure of a beam produced by the SAPT synchrotron. The radiation pulse duration time T1 is in the order of seconds [34], making it longer than the transit of ions across the chamber (the charge collection time Tc is approximately 95 ms for the ionization chamber investigated in this paper [31, 35]). According to Boag's theory, the proton pencil beam can be considered as a continuous beam and the collection efficiency f of the parallel plate ionization chamber for a continuous beam can be expressed as

$$f = \frac{1}{\left(1 + \xi^2/6\right)}, \tag{1}$$

$$\xi = \frac{kd^2q^{\frac{1}{2}}}{V}, \tag{2}$$

where k is a constant related to the gas composition, temperature, pressure, and humidity of the gas in the chamber ($k_{air} = 2.01 \times 10^7$ and $k_{N2} = 5 \times 10^6$ in a standard atmosphere [36, 37]), d is the distance between the two plane-parallel electrodes (units of m), and V is the applied voltage in the ionization chamber (units of V). q is the ionized charge density per unit volume in the irradiation volume (units of $Cm^{-3}s^{-1}$). The ionization chamber investigated in this work was a parallel plate monitor chamber manufactured by Pyramid Technical, Inc. [35]. The gap between the two parallel plane electrodes is 5 mm and the recommended applied voltage range is 1000–2000 V.

Collection efficiency of a monitor parallel plate ionization chamber in a proton pencil scanning beam

In this work, Boag's theory was applied to a proton pencil beam scanning system and the non-uniform distribution of charge density was considered as a Gaussian distribution to derive an analytical solution for calculating collection efficiency in the beam spot area.

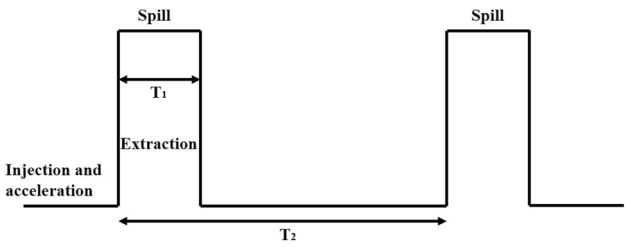

Fig. 1 Time structure of a beam produced by the SAPT synchrotron

In the proton pencil beam scanning apparatus of the SAPT facility, the beam monitor parallel plate ionization chambers are installed in the irradiation nozzle and the proton beam passes through the ionization chambers. The energy deposited per proton in the ionization chamber gap can be expressed as

$$\mathrm{d}E = \frac{\mathrm{d}E}{\mathrm{d}x} \cdot d, \tag{3}$$

where dE/dx is the stopping power of the gas media in the ionization chamber at a beam energy of E. This value can either be computed using the Bethe–Bloch formula or obtained experimentally. Therefore, the ionized charge density per unit volume q can be written as

$$q = J \cdot \left(\frac{\mathrm{d}E}{\mathrm{d}x}\right) \Big/ W, \tag{4}$$

where J is the surface current density (units of $Cm^{-2}s^{-1}$) and W is the mean energy required for beam particles to produce an electron–ion pair in the gas in the ionization chamber. $W = 34.2$ eV when the gas is air, and $W = 36.5$ eV when the gas is nitrogen [36].

Boag's theory assumes that ionized charge density is spatially uniform, which is applicable to passive scattering systems. However, in a pencil scanning beam, the transverse ionized charge density is non-uniform and can be assumed to follow a Gaussian distribution. The collection efficiency in a monitor parallel plate ionization chamber is also non-uniform in the pencil beam spot area. We rewrite collection efficiency as a function of x and y, which represent the two directions perpendicular to the proton beam direction. Formulas (1), (2), and (4) can be rewritten as

$$f(x,y) = \frac{1}{\left(1 + \xi^2(x,y)/6\right)}, \tag{5}$$

$$\xi(x,y) = \frac{kd^2q^{\frac{1}{2}}(x,y)}{V}, \tag{6}$$

$$q(x,y) = J(x,y) \cdot \left(\frac{\mathrm{d}E}{\mathrm{d}x}\right) \Big/ W. \tag{7}$$

The beam lateral distribution was considered as a standard Gaussian function. Therefore, $J(x,y)$ can be expressed as

$$J(x,y) = I \cdot G(x,y), \tag{8}$$

$$G(x,y) = \frac{1}{2\pi\sigma^2}\exp\left[-\left(\frac{x^2+y^2}{2\sigma^2}\right)\right], \tag{9}$$

where I represents the proton beam current intensity and G (x,y) is the transverse Gaussian distribution function of the proton beam with the standard deviation of σ.

We denote the generated charge as $Q_{\text{generated}}$ and the collected charge as $Q_{\text{collected}}$. Based on Formulas (5) to (9), $Q_{\text{generated}}$ and $Q_{\text{collected}}$ can be calculated as

$$Q_{\text{generated}} = \iint q(x,y)\mathrm{d}x\mathrm{d}y = \iint I \cdot G(x,y) \cdot \left(\frac{\mathrm{d}E}{\mathrm{d}x}\right) \Big/ W \mathrm{d}x\mathrm{d}y, \tag{10}$$

$$Q_{\text{collected}} = \iint f(x,y) \cdot q(x,y)\mathrm{d}x\mathrm{d}y = \iint f(x,y) \cdot I \cdot G(x,y) \cdot \left(\frac{\mathrm{d}E}{\mathrm{d}x}\right) \Big/ W \mathrm{d}x\mathrm{d}y. \tag{11}$$

Then, collection efficiency can be defined as

$$f_{\text{integral}} = \frac{Q_{\text{collected}}}{Q_{\text{generated}}} = \frac{\iint f(x,y) \cdot G(x,y)\mathrm{d}x\mathrm{d}y}{\iint G(x,y)\mathrm{d}x\mathrm{d}y}. \tag{12}$$

After setting the integral range R to $x^2 + y^2 \leq R^2$ (the integral range depends on the size of the ionization chamber; in this study, the monitor parallel plate ionization chamber was sufficiently large to cover the area of a pencil beam spot, so R was set to 5 σ), the pencil beam collection efficiency f_{integral} can be derived as

$$f_{\text{integral}} = m/n, \tag{13}$$

where

$$m = \frac{1}{T}\ln\left(\frac{T+1}{T\exp\left(\frac{-R^2}{2\sigma^2}\right)+1}\right),$$

$$n = 1 - \exp\left(\frac{-R^2}{2\sigma^2}\right),$$

$$T = \frac{A}{2\pi\sigma^2},$$

$$A = \frac{k^2 d^4 \cdot \left(\frac{\mathrm{d}E}{\mathrm{d}x}\right) I}{6V^2 W}.$$

The details of this derivation are presented in the Appendix. We call this collection efficiency calculation method the integral method. The collection efficiency f_{integral} represents the overall collection efficiency in the transverse distribution area of the pencil beam spot. In this study, we used f_{integral} to investigate the effects of beam parameters on collection efficiency.

From Formulas (5) to (9), it can be concluded that collection efficiency is not equal everywhere in the pencil beam spot area. The ionized charge density q, which is negatively correlated with collection efficiency, reaches its maximum value in the center of the pencil beam spot area. Therefore, the collection efficiency f_{center}, which is the collection efficiency at the center of the pencil beam spot, is the minimum collection efficiency in the area. We considered this specific scenario and calculated f_{center} as follows:

$$f_{\text{center}} = \frac{1}{\left(1 + \xi_{\text{center}}^2/6\right)}, \tag{14}$$

where

$$\xi_{\text{center}} = \frac{kd^2 q_{\text{center}}^{\frac{1}{2}}}{V},$$

$$q_{\text{center}} = J_{\text{center}} \cdot \left(\frac{\mathrm{d}E}{\mathrm{d}x}\right) \Big/ W,$$

$$J_{\text{center}} = \frac{1}{2\pi\sigma^2},$$

where J_{center} is the maximum surface current density, which is in the center of the Gaussian distribution. I represents the beam current intensity, and σ is the standard deviation of the proton pencil beam transverse Gaussian distribution.

3 Results

3.1 Applied voltage's effect on collection efficiency

Figure 2 presents saturation curves representing the collection efficiencies in 70.6, 150.4, and 235 MeV proton beams, where the solid, dashed, dashed-dotted, and dotted lines correspond to four beam current intensities of 0.3, 1, 3, and 5 nA, respectively. The beam sizes (σ) for all three energies were assumed to be 5 mm.

In Fig. 2, it is apparent that the collection efficiency increases with applied voltage when the beam current intensity is constant. One can also see that collection efficiency decreases with increasing beam current intensity (for example, in Fig. 2a, the collection efficiencies are 0.9980, 0.9934, 0.9806, and 0.9683 when the beam current intensities are 0.3, 1, 3, and 5 nA, respectively, where the applied voltage is 800 V). When comparing the saturation curves of the three energies with a beam current intensity of 3 nA and applied voltage of 800 V, the collection efficiencies are 0.9806 at 70.6 MeV, 0.9888 at 150.4 MeV, and 0.9916 at 235 MeV. Overall, collection efficiency is greater in a high-energy proton beam with a fixed applied voltage and beam current intensity. This is because high-energy protons deposit less energy in the monitor ionization chamber, resulting in lower ionized charge density.

We plotted a line representing a collection efficiency of 0.99 in Fig. 2 (red dashed line). One can see that the maximum applied voltage required is 1432 V when the collection efficiency is 0.99, where the proton beam energy is 70.6 MeV, beam current intensity is 5 nA, and beam size (σ) is 5 mm. Because the lowest energy rating of the 94 energetic proton beams in the SAPT facility is 70.6 MeV and the recommended applied voltage by Pyramid

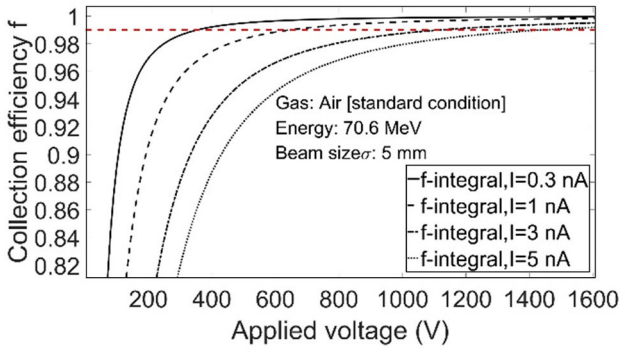

Fig. 2 Effects of applied voltage on ionization chamber collection efficiencies in three energetic proton beams: **a** 70.6, **b** 150.4, and **c** 235 MeV. The red dashed line represents a collection efficiency of 0.99

Technical, Inc. varies from 1000 to 2000 V, we used 1500 V as the standard applied voltage when studying the effects of other parameters on collection efficiency.

3.2 Effects of beam size on collection efficiency

The correlation between collection efficiency and beam size in 70.6 MeV proton beams was investigated. The results are presented in Fig. 3a, where the applied voltage is 1500 V. The solid, dashed, dashed-dotted, and dotted lines correspond to four beam current intensities of 0.3, 1, 3, and 5 nA, respectively. Figure 3a indicates that collection efficiency increases as beam size increases for a fixed beam current intensity. The beam size is 1.185 mm for a 0.3 nA beam current intensity and 4.724 mm for a 5 nA beam current intensity when the collection efficiency is 0.99. This demonstrates that to gain a constant collection efficiency with a fixed applied voltage, beam size should increase with beam current intensity.

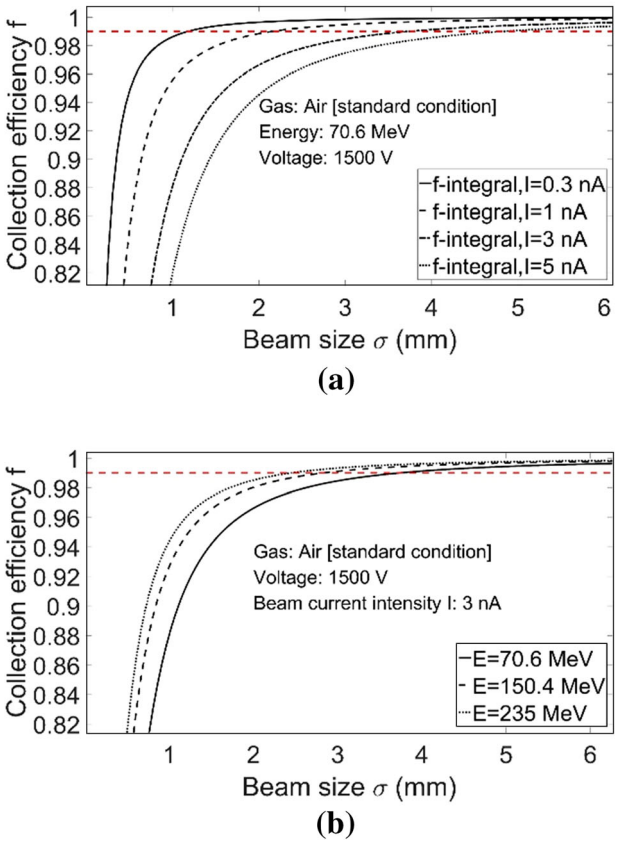

Fig. 3 Collection efficiency versus beam size for three proton beam energies. The red dashed line represents a collection efficiency of 0.99

In Fig. 3b, we compare the curves of collection efficiency for three energy proton beams with beam current intensity of a 3 nA. It can be seen that when collection efficiency, current intensity, and applied voltage are fixed, the beam size is smaller in a high-energy proton beam (beam size is 3.666 mm at 70.6 MeV, 2.871 mm at 150.4 MeV, and 2.383 mm in 235 MeV when the collection efficiency is 0.99). Furthermore, from Fig. 3b, it can be concluded that collection efficiency is positively related to beam energy when the other parameters are fixed.

3.3 Effects of beam current intensity and beam energy on collection efficiency

The relationships between collection efficiency and beam current intensity with a fixed beam size and applied

voltage for three proton beam energies are presented in Fig. 4a. One can see that in both Fig. 4a and formula (13), collection efficiency is inversely proportional to beam current intensity. Under the constraint that collection efficiency is at least 0.99, the maximum value of beam current intensity is 12.55 nA for the 235 MeV beam, which is greater than the values of 9.396 nA for the 150.4 MeV beam and 5.344 nA for the 70.6 MeV beam. The maximum value of beam current intensity is denoted as I_{max}. This value can be used as a reference value for maximum beam current intensity when the collection efficiency of the monitor ionization chamber is at least 0.99.

The conclusion can be drawn from Figs. 2, 3, and 4a that collection efficiency is positively related to applied voltage, beam size, and beam energy (or the inverse of dE/dx), and is negatively related to beam current intensity. To investigate the constraint of collection efficiency on beam current intensity at the SAPT facility, we simulated the beam sizes of 94 proton beam energies (varying from 70.6 MeV to 235 MeV) in the same position in a dose monitor ionization chamber using Monte Carlo simulation. Figure 4b presents the beam sizes (blue dotted line) and the inverse of stopping power (dE/dx, green dotted line) for the 94 proton beam energies. The collection efficiencies of the 94 proton beam energies with a beam current intensity of 3 nA are presented in Fig. 4c. With the combined influence of beam size and stopping power, collection efficiency decreases as beam energy increases owing to the dominant effect of beam size. Collection efficiency reaches a minimum value of 0.9947 when the beam energy is 154 MeV, then increases with increasing beam energy because the effect of stopping power is dominant.

The variation in collection efficiency is less than 0.0012 (maximum collection efficiency is 0.9959 at 70.6 MeV) in Fig. 4c, indicating that the effect of beam energy on collection efficiency can be regarded as negligible. It should be noted that this conclusion is based on the collection efficiency calculated from the beam size data presented in Fig. 4b. This conclusion may not be valid when the beam sizes of the 94 proton beam energies are small and fixed at the same value. For example, in Fig. 3b, the collection efficiencies of the 70.6 MeV and 235 MeV proton beams are 0.9853 and 0.9666, respectively, when the beam sizes, beam current intensities, and applied voltages are fixed as 3 mm, 3 nA, and 1500 V, respectively. The difference between the two collection efficiencies is 0.0187, which is non-negligible.

In Fig. 4d, we plot the I_{max} values of the 94 proton beam energies based on the data in Fig. 4b. The law of change for I_{max} with proton beam energy is consistent with the law of change for collection efficiency in Fig. 4c. These data can be used as a reference for the SAPT facility to determine the maximum value of beam current intensity that can

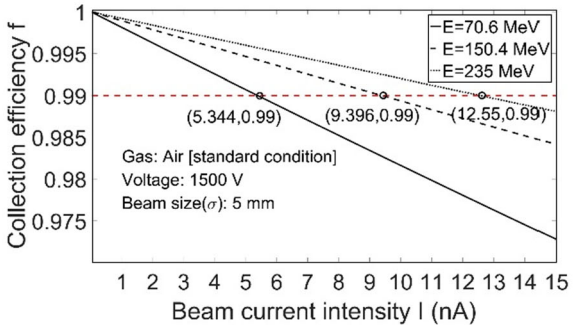

(a)

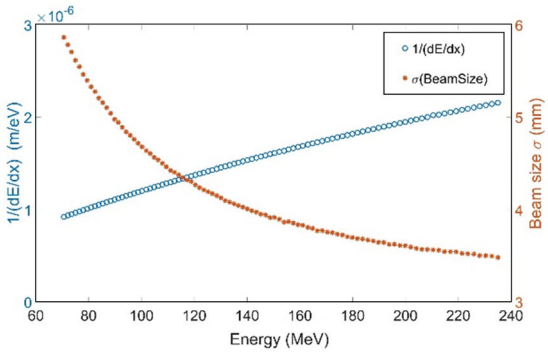

(b)

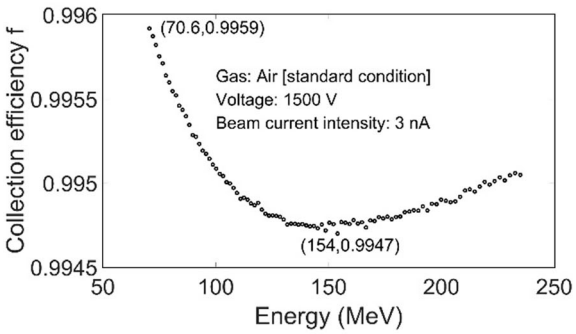

(c)

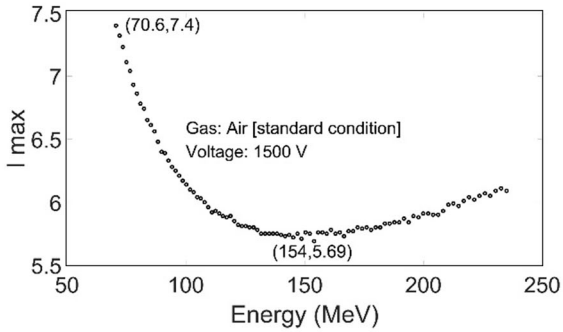

(d)

◀**Fig. 4** **a** Correlation between beam current intensity and efficiency for 70.6, 150.4, and 235 MeV proton beams. **b** Beam sizes and inverse of stopping powers for 94 proton beam energies. **c** Collection efficiency for 94 proton beam energies. **d** I_{max} values for 94 proton beam energies

be applied for each proton beam energy when the collection efficiency of the monitor ionization chamber is at least 0.99.

3.4 Effects of filling gas on collection efficiency

We replaced the filling gas in the ionization chamber with nitrogen (N_2) and calculated the resulting changes in collection efficiency. Figure 5 presents the collection efficiency of a 70.6 MeV, 5 nA proton beam. The solid and dotted lines represent the collection efficiencies of ionization chambers filled with air and nitrogen, respectively.

The collection efficiency with a 3 mm beam size and 5 nA beam current intensity increases from 0.9749 to 0.9983 when the filling gas is replaced with nitrogen, indicating that changing the filling gas from air to nitrogen can improve collection efficiency. This is because the constant k in formula (13) changes from 2.01×10^7 to 5×10^6 when the air is replaced with nitrogen.

4 Discussion

Collection efficiency is positively correlated with beam size and negatively correlated with beam current intensity when all other parameters are fixed. In other words, to ensure that the collection efficiency of a monitor parallel plate ionization chamber is no less than a certain value (in this study, we considered a value of 0.99), there should be constraints on beam current intensity and beam size. In pencil beam proton therapy, a smaller beam size can form a

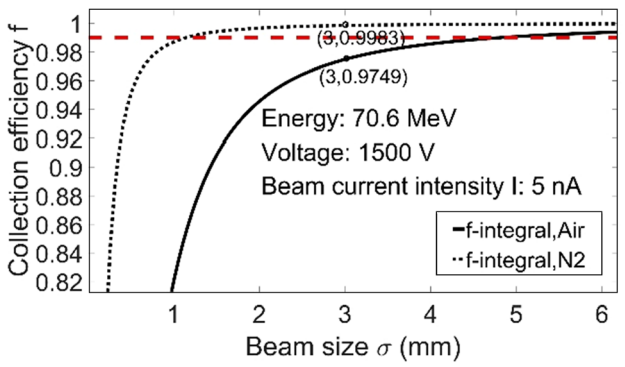

Fig. 5 Correlation between collection efficiency and beam size calculated in air and nitrogen. The red dashed line represents a collection efficiency of 0.99

smaller penumbra for the dose distribution, which can reduce the dose to OARs and normal tissue around the target. Additionally, treatment time can be reduced with a higher beam current intensity, which can improve the efficiency of treatment and reduce patient movement during treatment. Therefore, a balance between the accuracy of the monitor ionization chamber and beam parameters should be pursued.

Within the allowable voltage range of a monitor parallel plate ionization chamber, one can increase collection efficiency by increasing the applied voltage. This means that with increasing voltage, a smaller beam size and higher beam current intensity can be adopted in a pencil beam scanning system when the accuracy of the monitor ionization chamber is guaranteed. Furthermore, we determined that changing the filling gas from air to nitrogen will improve collection efficiency, which can improve the acceptability of smaller beam sizes and higher beam current intensities while maintaining collection efficiency.

The relationships between collection efficiency and beam energy, and between collection efficiency and beam size were investigated separately in this study. From Fig. 3b, we can draw the conclusion that collection efficiency is positively related to beam energy when the other parameters are fixed. As shown in Fig. 4b, the beam size at the position of the dose monitor ionization chamber is smaller for a high-energy proton beam. Based on the combined influence of beam size and energy, collection efficiency initially decreases with increasing beam energy. When the beam energy reaches 154 MeV, collection efficiency increases with beam energy. However, the overall variation in collection efficiency is less than 0.0012, as shown in Fig. 4c, which can be regarded as negligible. This is consistent with the conclusion presented by Mirandola [38] that the correlation between collection efficiency (caused by volume recombination) and beam energy is negligible for a pencil proton beam. However, it should be noted that the collection efficiency discussed in Mirandola's paper is the collection efficiency of a field ionization chamber, which was measured at different depths in a water phantom. The collection efficiency calculated in our study is the collection efficiency of a monitor ionization chamber, which is installed in an irradiation nozzle. The beam size is smaller at the position of the irradiation nozzle than at a position in a water phantom. The effects of beam energy on the collection efficiency of a monitor ionization chamber should be considered when the beam size is small.

In the final stage of this study, we compared $f_{integral}$ (solid line) and f_{center} (dotted line) values, as shown in Fig. 6. When 0.99 is used as the designated values for $f_{integral}$ and f_{center}, the applied voltages are 550 and 799 V, respectively. In other words, it is possible to guarantee a

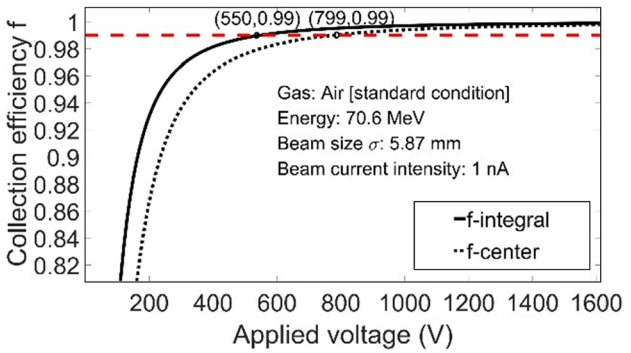

Fig. 6 Collection efficiency f_{integral} (solid line) and f_{center} (dotted line) values. The red dashed line represents a collection efficiency of 0.99

minimum collection efficiency greater than 0.99 in the pencil beam spot area when the applied voltage is at least 799 V and the other parameters are fixed. As mentioned in Sect. 2, the collection efficiency f_{integral} represents the overall collection efficiency in the pencil beam spot area, while f_{center} is the minimum collection efficiency in the pencil beam spot area. Therefore, f_{center} can be considered as the strictest constraint on applied voltage and beam parameters, such as beam size and beam current intensity.

5 Conclusions

In this study, we analyzed the collection efficiency of monitor parallel plate ionization. We applied Boag's theory to a proton pencil beam system and derived an analytical solution that considers the transverse distribution of charge density during ionization as a Gaussian function to calculate collection efficiency in the beam spot area.

This calculation method is useful for studying the effects of applied voltage, filling gas, and beam parameters, such as beam size, beam current intensity, and beam energy, on collection efficiency. It was determined that collection efficiency is positively correlated with applied voltage, beam size, and beam energy, but negatively correlated with beam current intensity. Additionally, changing the filling gas from air to nitrogen can improve collection efficiency when the other parameters are fixed.

Appendix. Derivation of integral collection efficiency

As shown in formula (12) in Sect. 2, the integral collection efficiency can be defined as

$$f_{\text{integral}} = \frac{Q_{\text{collected}}}{Q_{\text{generated}}} = \frac{\iint f(x,y)\cdot G(x,y)\mathrm{d}x\mathrm{d}y}{\iint G(x,y)\mathrm{d}x\mathrm{d}y} = \frac{m}{n}. \tag{A1}$$

Then, based on formulas (5) to (9), we can derive that

$$f(x,y) = \frac{1}{\left(1+\xi^2(x,y)/6\right)} = \frac{1}{1+\frac{k^2d^4\cdot q(x,y)}{6V^2}} = \frac{1}{1+\frac{k^2d^4\frac{\mathrm{d}_E}{\mathrm{d}_x}I\cdot G(x,y)}{6V^2W}}. \tag{A2}$$

Let $A = \frac{k^2d^4\frac{\mathrm{d}_E}{\mathrm{d}_x}I}{6V^2W}$. Then, $f(x,y)$ can reformulated as

$$f(x,y) = \frac{1}{1+A\cdot G(x,y)}, \tag{A3}$$

and

$$m = \iint f(x,y)\cdot G(x,y)\mathrm{d}x\mathrm{d}y = \iint \frac{G(x,y)}{1+A\cdot G(x,y)}\mathrm{d}x\mathrm{d}y = \iint \frac{\frac{1}{2\pi\sigma^2}\cdot\exp\left(-\frac{x^2+y^2}{2\sigma^2}\right)}{1+\frac{A}{2\pi\sigma^2}\cdot\exp\left(-\frac{x^2+y^2}{2\sigma^2}\right)}\mathrm{d}x\mathrm{d}y \tag{A4}$$

We define $T = \frac{A}{2\pi\sigma^2}$ and select the integral range of R (namely $x^2+y^2 \le R^2$). By using the polar transformation (i.e., $x = \rho\cdot\cos\theta, y = \rho\cdot\sin\theta$), the following formulas can be derived:

$$\begin{aligned} m &= \frac{1}{2\pi\sigma^2}\iint \frac{\exp\left(-\frac{x^2+y^2}{2\sigma^2}\right)}{1+T\cdot\exp\left(-\frac{x^2+y^2}{2\sigma^2}\right)}\mathrm{d}x\mathrm{d}y \\ &= \frac{1}{2\pi\sigma^2}\int_0^R\int_0^{2\pi} \frac{\exp\left(-\frac{\rho^2}{2\sigma^2}\right)}{1+T\cdot\exp\left(-\frac{\rho^2}{2\sigma^2}\right)}\rho\mathrm{d}\theta\mathrm{d}\rho \\ &= \frac{1}{T}\ln\left(\frac{T+1}{T\exp\left(\frac{-R^2}{2\sigma^2}\right)+1}\right) \end{aligned} \tag{A5}$$

$$n = \iint G(x,y)\mathrm{d}x\mathrm{d}y = \iint \frac{1}{2\pi\sigma^2}\cdot\exp\left(-\frac{x^2+y^2}{2\sigma^2}\right)\mathrm{d}x\mathrm{d}y = \frac{1}{2\pi\sigma^2}\int_0^R\int_0^{2\pi}\exp\left(-\frac{\rho^2}{2\sigma^2}\right)\rho d\theta d\rho = 1-\exp\left(\frac{-R^2}{2\sigma^2}\right) \tag{A6}$$

Finally, the integral collection efficiency can be written as

$$f_{\text{integral}} = m/n \tag{A7}$$

with

$$m = \frac{1}{T}\ln\left(\frac{T+1}{T\exp\left(\frac{-R^2}{2\sigma^2}\right)+1}\right),$$

$$n = 1 - \exp\left(\frac{-R^2}{2\sigma^2}\right),$$

$$T = \frac{A}{2\pi\sigma^2},$$

$$A = \frac{k^2 d^4 \cdot \left(\frac{\mathrm{d}E}{\mathrm{d}x}\right) I}{6V^2 W}.$$

References

1. R.R. Wilson, Radiological use of fast protons. Radiology **47**(5), 487–491 (1946). https://doi.org/10.1148/47.5.487
2. A.J. Lomax, Intensity modulation methods for proton radiotherapy. Phys. Med. Biol. **44**(1), 185–205 (1999). https://doi.org/10.1088/0031-9155/44/1/014
3. H. Paganetti, *Proton Therapy Physics* (CRC Press, Boca Raton, 2016), pp. 41–80. https://doi.org/10.1088/978-0-7503-1370-4
4. B.Q. Zhao, M.H. Zhao, M. Liu et al., The front-end electronics design of dose monitors for beam delivery system of Shanghai advanced proton therapy facility. Nucl. Sci. Tech. **28**(6), 83 (2017). https://doi.org/10.1007/s41365-017-0230-y
5. C. Miao, M. Liu, C. Yin et al., Precise magnetic field control of the scanning magnets for the APTRON beam delivery system. Nucl. Sci. Tech. **28**(12), 172 (2017). https://doi.org/10.1007/s41365-017-0324-6
6. Y.J. Jia, Y.J. Li, X. Zhang et al., Simulation of spot scanning in proton therapy. Nucl. Tech. **39**(9), 090202 (2016). https://doi.org/10.11889/j.0253-3219.2016.hjs.39.090202. **(in Chinese)**
7. C.P. Karger, O. Jakel, H. Palmans et al., Dosimetry for ion beam radiotherapy. Phys. Med. Biol. **55**(21), 193–234 (2010). https://doi.org/10.1088/0031-9155/55/21/R01
8. S. Giordanengo, H. Palmans, Dose detectors, sensors, and their applications. Med. Phys. **45**(11), e1051–e1072 (2018). https://doi.org/10.1002/mp.13089
9. G. Magro, S. Molinelli, A. Mairani et al., Dosimetric accuracy of a treatment planning system for actively scanned proton beams and small target volumes: Monte Carlo and experimental validation. Phys. Med. Biol. **60**(17), 6865–6880 (2015). https://doi.org/10.1088/0031-9155/60/17/6865
10. M. Marrale, A. Carlino, S. Gallo et al., EPR/alanine dosimetry for two therapeutic proton beams. Nucl. Instrum. Meth. B **368**(368), 96–102 (2016). https://doi.org/10.1016/j.nimb.2015.12.022
11. P. Andreo, D. Burns, K. Hohlfeld et al., *Absorbed Dose Determination in External Beam Radiotherapy: An International Code of Practice for Dosimetry Based on Standards of Absorbed Dose to Water* (International Atomic Energy Agency, Vienna, 2000)
12. International Commission on Radiation Units and Measurements, The dosimetry of pulsed radiation. (ICRU Report 34, Bethesda, 1982)
13. P.R. Almond, P.J. Biggs, B.M. Coursey et al., AAPM's TG-51 protocol for clinical reference dosimetry of high-energy photon and electron beams. Med. Phys. **26**(9), 1847–1870 (1999). https://doi.org/10.1118/1.598691
14. J.W. Boag, in *Ionization Chambers Radiation Dosimetry (Instrumentation vol II)*, 2nd edn (Academic, New York, 1966), Chapter 9
15. G. Jaffe, Zur theorie der ionisation in kolonnen. Ann. Phys. **347**(12), 303–344 (1913). https://doi.org/10.1002/andp.19133471205
16. E. Kara-Michailova, D.E. Lea, The interpretation of ionization measurements in gases at high pressures. Proc. Cambridge Phil. Soc. **36**(1), 101–126 (1940). https://doi.org/10.1017/S0305004100017059
17. T. Kanai, M. Sudo, N. Matsufuji et al., Initial recombination in a parallel-plate ionization chamber exposed to heavy ions. Phys. Med. Biol. **43**(12), 3549–3558 (1998). https://doi.org/10.1088/0031-9155/43/12/012
18. J.W. Boag, T. Wilson, The saturation curve at high ionization intensity. British J. Appl. Phys. **3**(7), 222–229 (1952). https://doi.org/10.1088/0508-3443/3/7/305
19. P.J. Biggs, I.P. Nogueira, Measurement of the collection efficiency of a large volume spherical ionization chamber in megavoltage therapy beams. Med. Phys. **26**(10), 2107–2112 (1999). https://doi.org/10.1118/1.598726
20. F. Deblois, C. Zankowski, E.B. Podgorsak, Saturation current and collection efficiency for ionization chambers in pulsed beams. Med. Phys. **27**(5), 1146–1155 (2000). https://doi.org/10.1118/1.598992
21. R.F. Laitano, A.S. Guerra, M. Pimpinella et al., Charge collection efficiency in ionization chambers exposed to electron beams with high dose per pulse. Phys. Med. Biol. **51**(24), 6419–6436 (2006). https://doi.org/10.1088/0031-9155/51/24/009
22. H. Palmans, F. Verhaegen, J.-M. Denis et al., Dosimetry using plane-parallel ionization chambers in a 75 MeV clinical proton beam. Phys. Med. Biol. **47**(16), 2895–2905 (2002). https://doi.org/10.1088/0031-9155/47/16/305
23. H. Palmans, R. Thomas, A. Kacperek, Ion recombination correction in the Clatterbridge Centre of Oncology clinical proton beam. Phys. Med. Biol. **51**(4), 903–917 (2006). https://doi.org/10.1088/0031-9155/51/4/010
24. S. Lorin, E. Grusell, N. Tilly et al., Reference dosimetry in a scanned pulsed proton beam using ionisation chambers and a Faraday cup. Phys. Med. Biol. **53**(13), 3519–3529 (2008). https://doi.org/10.1088/0031-9155/53/13/008
25. S. Rossomme, J. Hopfgartner, N.D. Lee et al., Ion recombination correction in carbon ion beams. Med. Phys. **43**(7), 4198–4208 (2016). https://doi.org/10.1118/1.4953637
26. S. Rossomme, J. Horn, S. Brons et al., Ion recombination correction factor in scanned light-ion beams for absolute dose measurement using plane-parallel ionisation chambers. Phys. Med. Biol. **62**(13), 5365–5382 (2017). https://doi.org/10.1088/1361-6560/aa730f
27. M. Liszka, L. Stolarczyk, M. Klodowska et al., Ion recombination and polarity correction factors for a plane–parallel ionization chamber in a proton scanning beam. Med. Phys. **45**(1), 391–401 (2018). https://doi.org/10.1002/mp.12668
28. R. Tansho, T. Furukawa, Y. Hara et al., Experimental verification of gain drop due to general ion recombination for a carbon-ion pencil beam. Med. Phys. **43**(2), 635–642 (2016). https://doi.org/10.1118/1.4939225
29. L. Karsch, Derivation of a formula describing the saturation correction of plane-parallel ionization chambers in pulsed fields with arbitrary repetition rate. Phys. Med. Biol. **61**(8), 3222–3236 (2016). https://doi.org/10.1088/0031-9155/61/8/3222
30. J.B. Christensen, H. Tolli, N. Bassler, A general algorithm for calculation of recombination losses in ionization chambers exposed to ion beams. Med. Phys. **43**(10), 5484–5492 (2016). https://doi.org/10.1118/1.4962483
31. International Commission on Radiation Units and Measurements, *Prescribing, Recording, and Reporting Proton-Beam Therapy.* (ICRU Report 78, Bethesda, MD, 2007), p. 71

32. Y.Q. Ge, C.X. Yin, Z. Li et al., Optimization design of a multi-layer ionization chamber. Nucl. Tech. **42**(6), 060202 (2019). https://doi.org/10.11889/j.0253-3219.2019.hjs.42.060202. **(in Chinese)**
33. M. Gillin, N. Sahoo, M. Bues et al., Commissioning of the discrete spot scanning proton beam delivery system at the University of Texas M.D. Anderson Cancer Center, Proton Therapy Center, Houston. Med. Phys. **37**(1), 154–163 (2009). https://doi.org/10.1118/1.3259742
34. Y. Yang, M. Zhang, D. Li, Simulation study of slow extraction for the Shanghai advanced proton therapy facility. Nucl. Sci. Tech. **28**(9), 120 (2017). https://doi.org/10.1007/s41365-017-0273-0
35. Integrated Dosimetry and Position Sensing Ionization Chamber with Dual Redundant Dose Measurement (Pyramid Technical Consultants, Inc., 2019), http://www.ptcusa.com/files/datasheet/IC128-25LC-2I_DS_190605.pdf
36. J.R. Green, Saturation characteristics of parallel-plate ionization chambers. Phys. Med. Biol. **9**(2), 143–154 (1964). https://doi.org/10.1088/0031-9155/9/2/302
37. K. Katoh, J.R. Greening, CORRESPONDENCE: on Greening's treatment of saturation characteristics of parallel-plate ionization chambers. Phys. Med. Biol. **10**(4), 565–566 (1965). https://doi.org/10.1088/0031-9155/10/4/413
38. A. Mirandola, G. Magro, D. Maestri et al., Determination of ion recombination and polarity effect correction factors for a plane-parallel ionization Bragg peak chamber under proton and carbon ion pencil beams. Phys. Med. Biol. **64**(9), 095010 (2019). https://doi.org/10.1088/1361-6560/ab0db4